OUTER SCALING OF ROUGH AND SMOOTH WALL BOUNDARY LAYERS UNDER ADVERSE PRESSURE GRADIENT CONDITIONS

Ralph J. Volino
Department of Mechanical and Nuclear Engineering
United States Naval Academy
Annapolis, Maryland, 21402, USA
volino@usna.edu

Michael P. Schultz
Department of Naval Architecture and Ocean Engineering
United States Naval Academy
Annapolis, Maryland, 21402, USA
mschultz@usna.edu

ABSTRACT

Experiments were conducted in adverse pressure gradient (APG) boundary layers over rough and smooth walls. Cases were considered with various pressure gradient strengths and upstream conditions. Profiles of mean velocity and turbulence quantities were measured at multiple streamwise stations to document the response of the flow to the APG. The data suggest that an APG causes attached turbulent eddies to become detached, and motivates the proposal of a new scaling to collapse the data in the outer part of the boundary layer. The distance from the wall is normalized as $y^*=(y - a\delta^*)/(\delta - a\delta^*)$ where δ, δ^* and a=1.1 are the boundary layer thickness, displacement thickness, and an empirical constant, respectively. Velocity is scaled using the friction velocity at the start of the APG region. Data from all cases in which an APG is imposed on a canonical zero pressure gradient (ZPG) boundary layer show good collapse of the mean velocity and Reynolds stress profiles with the new scaling. For a case in which an APG followed directly after a favourable pressure gradient (FPG), the initial development of the boundary layer was changed, but after some distance the new scaling again collapsed the profiles.

INTRODUCTION

Canonical zero pressure gradient boundary layers have been well studied on both smooth and rough surfaces, as described in reviews such as Chung et al. (2021). Outside a few roughness heights of the wall, Townsend (1976) indicated that smooth- and rough-wall boundary layers are similar if scaled using the boundary layer thickness, δ, and friction velocity, u_τ. Many studies have verified this similarity. For non-zero pressure gradients, however, scaling with δ and u_τ does not result in similarity either in the streamwise direction or between rough- and smooth-wall cases with the same freestream velocity distribution. This is particularly true for adverse pressure gradients, as shown in studies such as Volino and Schultz (2022).

Several studies have considered the scaling of smooth-wall APG flows. Some noted that u_τ is not an appropriate velocity scale because it goes to zero as a boundary layer approaches separation, giving the misleading impression that the Reynolds stresses are growing rapidly (e.g. Maciel et al., 2006; Harun et al., 2013; Romero et al., 2022). Maciel et al. (2006) found that the Zagarola and Smits (1998) velocity scale, $U_{ZS}=U_e\delta^*/\delta$, where U_e is the freestream velocity and δ^* is the displacement thickness, is useful for collapsing mean velocity profiles in defect coordinates, but does not result in similarity for the Reynolds stresses. Wu and Piomelli (2018) observed the same for rough-wall boundary layers. Aubertine and Eaton (2005) found that the maximum U_e in their boundary layer, which occurred at the start of the APG, worked well for normalizing the Reynolds stresses in the outer region. They noted that the APG boundary layer was in a non-equilibrium state since the outer flow profiles collapsed using a constant for normalizing instead of the local U_e or u_τ. Han et al. (2024) proposed a modification to the Zagarola and Smits scaling for APG cases. For scaling the mean velocity they used

$$U_{ZS-apg} = U_{ZS}\left(1 - H\frac{\delta}{U_e}\frac{dU_e}{dx}\right), \tag{1}$$

where x is the streamwise coordinate and H is the shape factor (ratio of displacement and momentum thickness). For scaling the Reynolds shear stress and the wall-normal component of the Reynolds normal stress, $\overline{v'^2}$, they used

$$uv_{ZS-apg} = U_e U_{ZS-apg}. \tag{2}$$

For the streamwise component, $\overline{u'^2}$, the scaling velocity was

$$uu_{ZS-apg} = uv_{ZS-apg} - HU_e u_\tau. \tag{3}$$

These scalings worked well for the smooth-wall APG cases tested.

The APG boundary layer structure was considered by Yoon et al. (2020) and Gungor et al. (2022), who reported that detached eddies become dominant far from the wall, but that these eddies originate as attached eddies farther upstream.

Most studies used δ as their length scale. For strong APG cases with inflection points in the mean velocity profile, Schatzman and Thomas (2017) proposed using

$$\delta_w = (U_e - U_{IP})\left(\frac{dU}{dy}\right)_{IP}, \tag{4}$$

where U is the local mean velocity, y is the distance from the wall, and IP indicates the location of the farthest inflection point from the wall. For their velocity scale they used

$$U_d = U_e - U_{IP}. \tag{5}$$

As the boundary layer approached separation, the intent was to choose parameters that represented the size and velocity associated with the shear layer forming in the outer flow. The scaling worked well for both the mean velocity and Reynolds stresses.

The objective of the present work is to find velocity and length scales that will collapse mean velocity and Reynolds stress profiles in the outer region for ZPG to strong APG conditions on both smooth and rough walls. Experiments were conducted under a range of APG conditions. The scaling that provided the best results is presented below.

EXPERIMENTS

Experiments were conducted in the recirculating water tunnel described in Volino (2020). Water entered the test section through a honeycomb and screens followed by a three-dimensional contraction. The test section was 0.2 m wide, nominally 0.1 m tall at the entrance, and 2 m long. The lower surface of the test section was the test wall. For smooth-wall cases, an acrylic plate was used. For rough-wall cases, a plate was made through additive manufacturing with mathematically generated, three-dimensional, random roughness. The rms, maximum peak to trough, and equivalent sandgrain roughness heights, skewness, and effective slope were 0.35 mm, 3.5 mm, 1.7 mm, 0.98, and 0.4, respectively. Details are available in Volino and Schultz (2022). The upper surface of the test section consisted of four flat plates that could be positioned to set the desired streamwise pressure gradient. The side walls were transparent for optical access. The freestream velocity at the inlet of the test section was set to 1 m/s for the cases considered, and was equal to 2 m/s at the start of the APG region. The freestream turbulence level was 0.3%

Experimental cases are used from Volino (2020) and Volino and Schultz (2022) with smooth and rough test walls, respectively, along with two new cases. Conditions for the cases are provided in Table 1, where the subscript o denotes the value at the beginning of the APG. Schematics of the test section are shown in Fig. 1. The acceleration parameter, $K=(\nu/U_e^2)(dU_e/dx)$, was approximately constant for cases 1-6 with the average value given in Table 1. For cases 7 and 8 the K distribution is shown in Fig. 2. In all cases x=0 denotes the start of the APG. The Clauser pressure gradient parameter, $\beta=-(\delta^* U_e/u_\tau^2)(dU_e/dx)$, is also shown in Fig. 2, with the maximum value for each case listed in Table 1. In cases 1-7, the flow was subject to a favourable pressure gradient followed by a return to canonical conditions in a ZPG region, which in turn was followed by the APG region of interest. In case 7 an FPG sink flow with K=1×10^{-6} was followed immediately by the APG region with no ZPG recovery.

Velocity profiles were acquired using the two-component LDV system described in Volino and Schultz (2022) at the spanwise centreline of the test section. The flow was seeded with 2 mm diameter silver coated glass spheres. The probe volume was 45 μm in diameter and 340 μm in length. It was traversed from the wall to the freestream at each streamwise station. At each location in the profile, data were acquired for 10000 large eddy turnover times. The streamwise locations of the profiles in cases 1-6 were x = -0.055, 0.083, 0.140, and 0.206 m. For cases 7 and 8 the stations locations are shown in Fig. 2. The friction velocity was determined at each station using the mean streamwise velocity and Reynolds shear stress profiles, as described in Volino and Schultz (2018).

Table 1. Flow parameters.

Case	Wall	K_{ave} ×10^7	β_{max}	$Re_{\theta o}$	$Re_{\tau o}$	H_o	H_{max}
1	S	-5	6.6	3285	1125	1.41	1.68
2	S	-2.5	1.0	3000	1052	1.39	1.45
3	S	-1.25	0.5	3371	1098	1.40	1.42
4	R	-5	63	5965	2407	1.69	2.44
5	R	-2.5	1.9	5059	2016	1.68	1.75
6	R	-1.25	0.7	5274	1970	1.64	1.66
7	R	-3.1	22	6133	2597	1.69	2.51
8	S	-3.9	4.7	1255	812	1.30	1.80

Cases 1-3, Volino (2020); 2-4, Volino and Schultz (2022); 7-8, present study. R=rough, S=smooth.

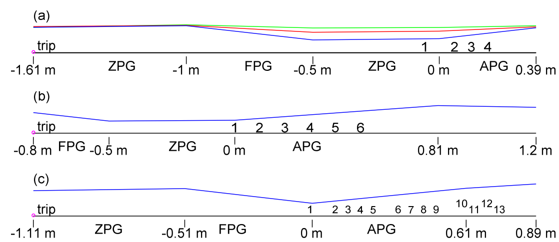

Figure 1. Cross section of test section in the streamwise-wall normal plane, approximately to scale. Numbers in test section indicate streamwise measurement stations: a) Blue ceiling for cases 1 and 4, red for 2 and 5, green for 3 and 6; b) Case 7; c) Case 8.

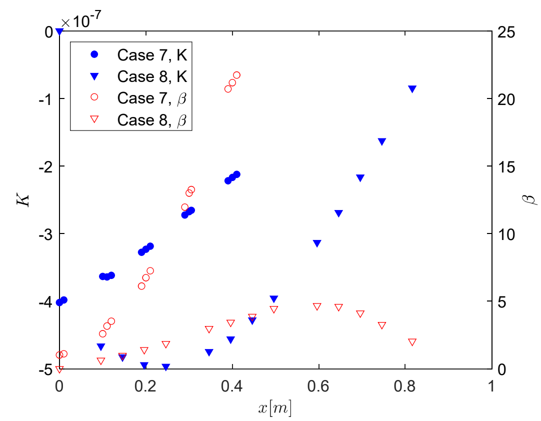

Figure 2. Acceleration parameter, K, and Clauser pressure gradient parameter, β, for cases 7 and 8.

RESULTS

The scaling quantities described above were tried with the present results in attempts to collapse the data in the outer boundary layer. Note that "outer" here refers to the wake region, not the entire region outside any roughness sublayer. Zagarola and Smits (1998) scaling worked well for collapsing the mean velocity profiles in defect coordinates, but as noted in Maciel et al. (2006) did not collapse the Reynolds stresses. Using U_{eo} as the velocity scale, as proposed by Aubertine and Eaton (2005) was helpful for collapsing the peak magnitudes of the Reynolds stresses in the smooth-wall cases, but not in the rough-wall cases. Using $u_{\tau o}$ instead was more helpful, but the scaling still did not account for shift of the peaks to larger y/δ with the APG. The scaling of Schatzman and Thomas (2017) was useful for smooth-wall profiles with inflection points, but did not collapse the rough-wall case profiles or the smooth-wall profiles from stations upstream of the development of an inflection point. The modified Zagarola and Smits scaling proposed by Han et al. (2024) worked well in collapsing the mean velocity for all of the present cases, and as in Han et al. (2024) it collapsed the Reynolds stresses for the smooth-wall cases. It did not collapse the Reynolds stresses for the rough-wall cases, and a replacement of U_e with u_τ in the scaling quantities did not help.

None of the previous scaling quantities provided fully satisfactory results. To suggest more appropriate scaling parameters, the spectra of the Reynolds shear stress for case 7 are shown in Fig. 3. At the first station, which is at the end of the ZPG region, the spectral peak extends from the wall out into the boundary layer, and the frequencies at all distances from the wall are similar. This suggests attached eddies, and that the turbulence in the outer region is generated or at least influenced by the near wall flow. As the flow moves downstream, the peak moves to higher y/δ, and the connection to the wall is weakened. The magnitude and dimensionless frequencies of the outer peak do not change greatly, but the near wall values drop. The results suggest that the outer region eddies have become largely detached, in agreement with Yoon et al. (2020) and Gungor et al. (2022), so that the local u_τ and δ are no longer the appropriate scaling values.

Since the outer region turbulence appears to be generated upstream while the boundary layer is still attached, perhaps the appropriate scaling velocity is the $u_{\tau o}$ value at the beginning of the APG. This is similar to the argument of Aubertine and Eaton (2005), but using $u_{\tau o}$ instead of U_{eo} accounts for the effect of roughness producing higher Reynolds stresses. The appropriate scaling length may be the distance from the boundary layer edge to some displacement from the wall that occurs as the APG begins to induce separation. This is taken as

$$\delta_d = \delta - a\delta^* \tag{6}$$

where a is a constant. The dimensionless distance from the wall is set as

$$y^* = (y - a\delta^*)/\delta_d \tag{7}$$

A value of a=1.1 was found empirically to best collapse the results.

Figure 4 shows the mean streamwise velocity in defect coordinates for all stations of cases 1-7. The collapse in the outer region is good, and the differences between cases is of the order of the uncertainty in the data. Figure 5 shows profiles of the Reynolds stresses. Collapse is again good in the outer region. Differences are clear in the inner region, due to the effects of pressure gradient and roughness. The collapse for the streamwise component of the Reynolds normal stress in Fig. 5a is not quite as good, which may indicate that the present scaling works best for active turbulent motions.

Figure 6 shows that the new scaling does not work as well for the higher order moments, in this case the triple product $-\overline{u'v'^2}$. The locations of the peaks do align, and the rough-wall cases collapse, but the smooth-wall cases do not and are lower than those for the rough wall. Since the triple products

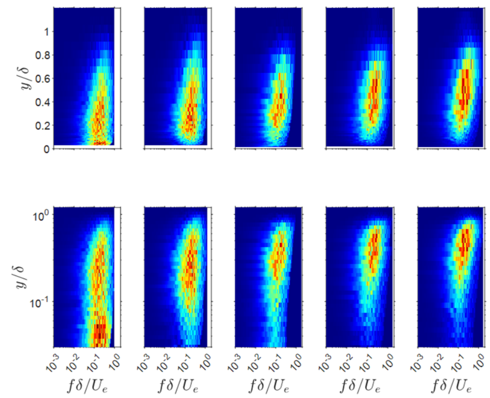

Figure 3. Premultiplied Reynolds shear stress spectra for case 1. Columns for streamwise stations 1-5. Row 1, y/δ linear scale; row 2, y/δ logarithmic scale. Spectra normalized with $u_{\tau o}^2$, same colour range for all plots. f is frequency.

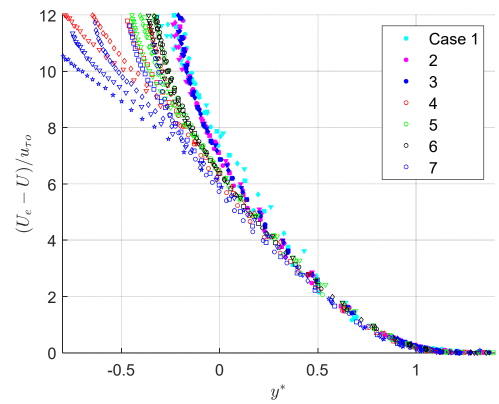

Figure 4. Mean velocity profiles in defect coordinates. Symbol colour indicates case from Table 1. Symbol shape indicates streamwise station: 1○, 2□, 3◊, 4▽, 5☆.

can be interpreted as transport terms for the Reynolds stresses, the differences in Fig. 6 may again indicate differences between active and inactive motions. The production terms for the Reynolds stresses, interestingly, do collapse in the outer region, as shown in Fig. 7.

Figure 8 shows the premultiplied spectra of Fig. 3 normalized using $u_{\tau o}$ and δ_d. Results are shown for y^*=0, which is approximately the location of the peak magnitude. All stations of case 7 (rough-wall) collapse, and the stations of case 1 (smooth-wall) also agree.

History Effects

Cases 1-7 all have a transition from canonical ZPG condition to an APG. The behaviour in the APG is different when the upstream conditions are changed. Figure 9 shows the mean velocity and Reynolds shear stress profiles for case 8, which has an immediate transition from an FPG to an APG. The friction velocity at the junction between the FPG and APG (x=0) is used for normalizing. The profiles are clearly different than those of Figs. 4 and 5, and do not collapse. The profile at the first station is typical of an FPG, with a low velocity deficit and reduced turbulence in boundary layer. The friction

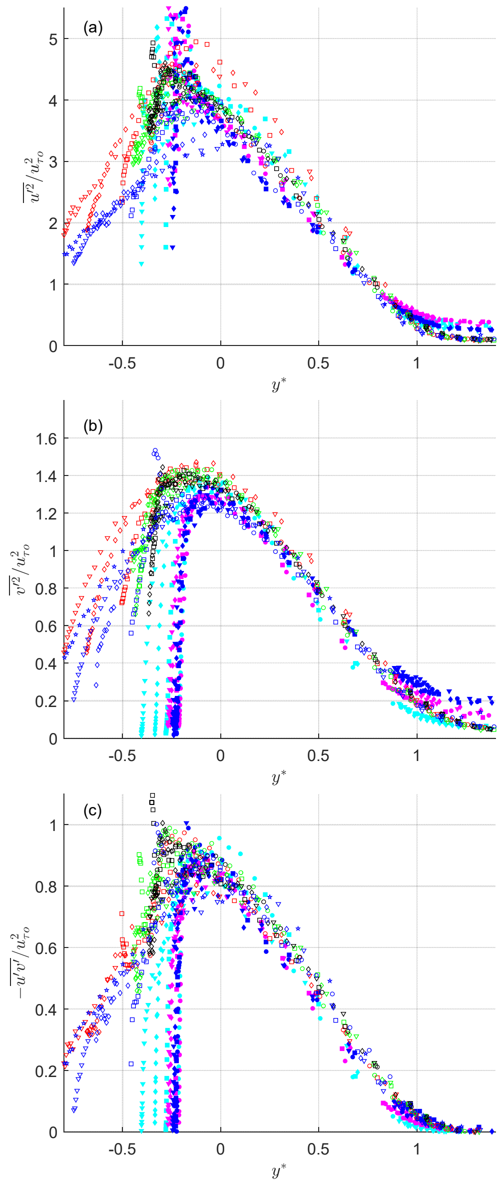

Figure 5. Reynolds stress profiles: a) $\overline{u'^2}$ (streamwise), b) $\overline{v'^2}$ (wall-normal), c) $-\overline{u'v'}$. symbols as in Fig. 1.

velocity is higher at this station than in the cases with a ZPG region, due to the high shear caused by the FPG. The result is profiles that lie significantly below those of Figs. 4 and 5.

Spectra for case 8 are shown in Fig. 10 in the same format as Fig. 3. As in the previous cases, the peak in the turbulence moves away from the wall in the APG region and eventually becomes detached from the wall. At the upstream stations, however, the link to the wall appears to persist longer than observed in Fig. 3. The FPG results in a thinner boundary layer with lower velocity deficit than in the cases with a ZPG region. The lower velocity deficit mitigates the initial effect of the APG and delays the detachment of the eddies. It is only at about the fifth station (x=0.35 m) in Fig. 10 that the spectra appear to detach as much as at the second station (x=0.1 m) in Fig. 3. The delay in the eddy detachment suggests that the appropriate scaling velocity should be taken somewhat downstream of the start of the APG. With $u_{\tau 2}$ set to the value

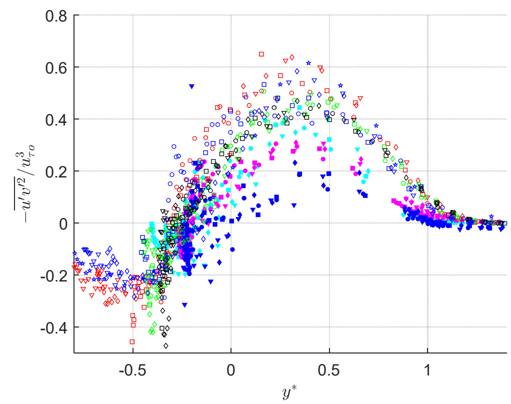

Figure 6. $-\overline{u'v'^2}$ profiles, symbols as in Fig. 1.

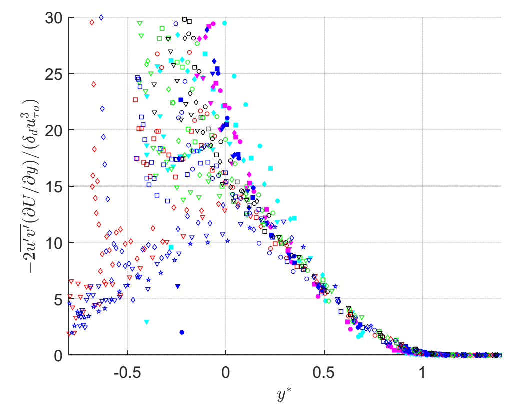

Figure 7. Primary production term for $\overline{u'^2}$ profiles, symbols as in Fig. 1.

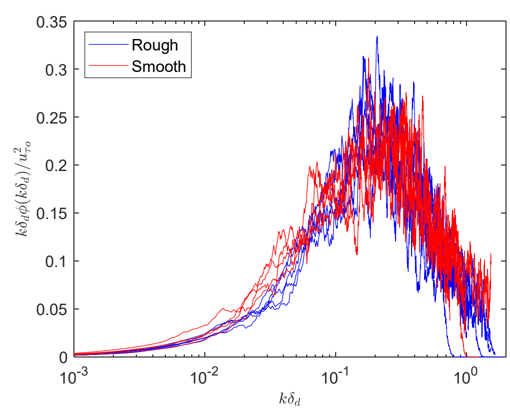

Figure 8. Premultiplied Reynolds shear stress spectra at y^*=0 for all streamwise stations of case 7 (blue) and case 1 (red). k is wavenumber.

of u_τ at the second station, the resulting defect velocity and Reynolds shear stress profiles are shown in Fig. 11. The profiles change for the first four or five stations, but downstream of this they collapse and agree with those of Figs. 4 and 5. Spectra at y^*=0 are shown in Fig. 12 in the format of Fig. 8. The wavenumber of the peak increases through the first five stations, in agreement with the changing profiles of Fig. 11. Farther downstream, however, the spectra collapse, again

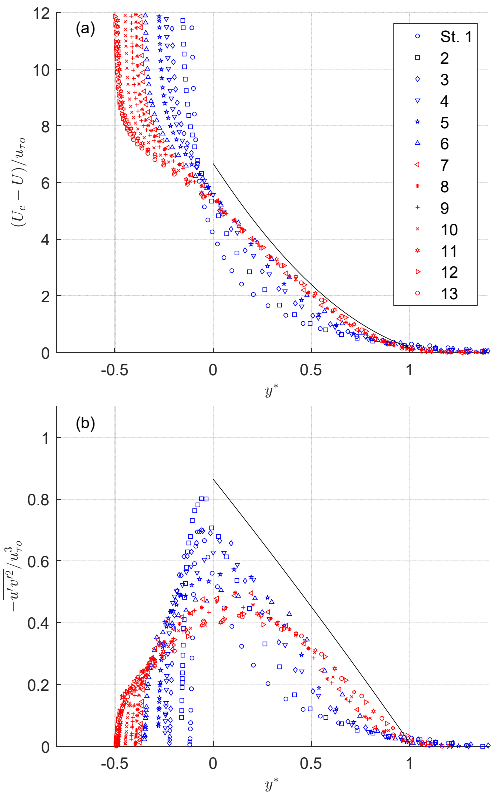

Figure 9. Profiles for case 8: a) Mean velocity defect, b) Reynolds shear stress. Quantities normalized with $u_{\tau o}$. Black lines are curve fits of data from Figs. 4 and 5c.

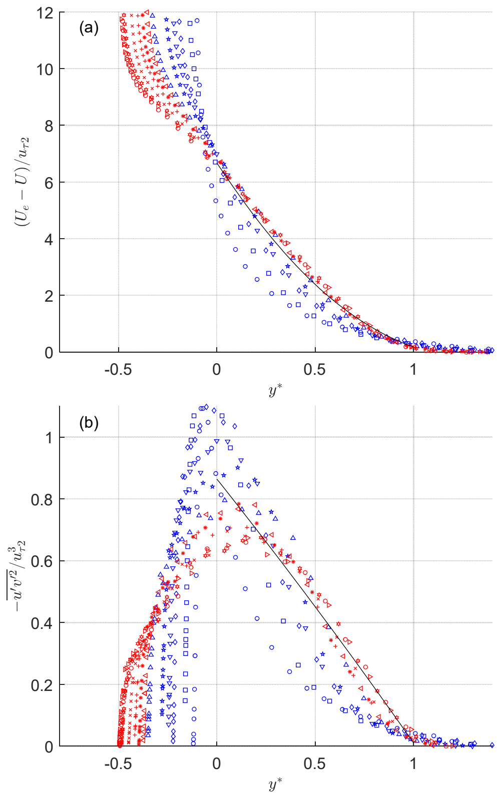

Figure 11. Profiles for case 8: a) Mean velocity defect, b) Reynolds shear stress. Quantities normalized with $u_{\tau 2}$. Black lines are curve fits of data from Figs. 4 and 5c. Symbols as in Fig. 9.

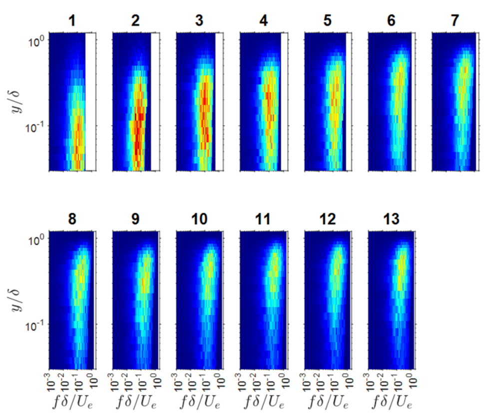

Figure 10. Premultiplied Reynolds shear stress spectra for case 8. Numbers indicate streamwise station. Spectra normalized with $u_{\tau 2}^2$, same colour range for all plots.

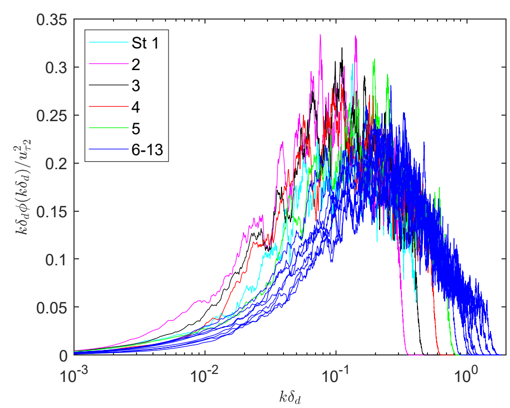

Figure 12. Premultiplied Reynolds shear stress spectra at y^*=0 for all streamwise stations of case 8.

in agreement with the collapse of the profiles in Fig. 11. Comparison of the spectra at the downstream stations to Fig. 8 shows agreement in both the wavenumber and magnitude of the peaks.

It appears that the upstream history affects the development of the boundary layer in the APG region, including the distance required for detachment of the turbulent eddies from the near wall region. Once the detachment occurs, however, the wake region appears to be similar in all cases when normalized with a friction velocity taken near the location where communication with the near wall region begins to be reduced.

CONCLUSIONS

Data from the literature and the present study indicate that turbulent eddies in the outer boundary layer begin to lose their connection to the near wall region in APG flows, such that scaling with local velocities and the boundary layer thickness begin to lose meaning. A new scaling that uses the upstream friction velocity, $u_{\tau o}$, and the local value of δ-1.1δ^* is proposed, and shown to result in good collapse of mean velocity and Reynolds stress profiles, and turbulence spectra in the outer part of the boundary layer for a range of APG strengths in both smooth- and rough-wall cases. The results suggest that the wake region of the boundary layer, as described by Coles (1956) with his universal wake function, is displaced from the wall in an APG, but is otherwise not greatly changed. The growth of the boundary layer and the detachment of the eddies from the near wall region are affected by the boundary layer history upstream of the APG region. A strong FPG upstream of an APG region reduces the velocity deficit and delays the detachment of the eddies at the start of the APG. If a u_τ value from downstream of the start of the APG is used for normalizing, however, collapse of the mean velocity profiles and Reynolds stresses can still be achieved.

REFERENCES

Aubertine, C. D., and Eaton, J. K., 2005, "Turbulence development in a non-equilibrium turbulent boundary layer with mild adverse pressure gradient", *Journal of Fluid Mechanics*, Vol. 532, pp. 345-364.

Chung, D., Hutchins, N., Schultz, M. P., and Flack, K. A., 2021, "Predicting the Drag of Rough Surfaces", *Annual Review of Fluid Mechanics*, Vol. 53, pp. 439-471.

Coles, D., 1956, "The law of the wake in the turbulent boundary layer", *Journal of Fluid Mechanics*, Vol. 1, pp. 191-226.

Gungor, T. R., Maciel, Y., and Gungor, A. G., 2022, "Energy transfer mechanisms in adverse pressure gradient turbulent boundary layers: production and inter-component redistribution", *Journal of Fluid Mechanics*, Vol. 948, A5.

Han, M., Ma, M., and Yan, C., 2024, "Consistent outer scaling and analysis of adverse pressure gradient turbulent boundary layers", *Journal of Fluid Mechanics*, Vol. 982, A17.

Harun, Z., Monty, J. P., Mathis, R., and Marusic, I., 2013, "Pressure gradient effects on the large-scale structure of turbulent boundary layers", *Journal of Fluid Mechanics*, Vol. 715, pp. 477-498.

Maciel, Y., Rossignol, K.-S., and Lemay, J., 2006, "Self-Similarity in the Outer Region of Adverse-Pressure-Gradient Turbulent Boundary Layers", *AIAA Journal*, Vol. 44, pp. 2450-2464.

Romero, S., Zimmerman, S., Philip, J., White, C., and Klewicki, J., 2022, "Properties of the inertial sublayer in adverse pressure-gradient turbulent boundary layers", *Journal of Fluid Mechanics*, Vol. 937, A30.

Schatzman, D. M., and Thomas, F. O., 2017, "An experimental investigation of an unsteady adverse pressure gradient turbulent boundary layer: embedded shear layer scaling", *Journal of Fluid Mechanics*, Vol. 815, pp. 592-642.

Townsend, A. A., 1976, *The Structure of Turbulent Shear Flow*, 2nd Ed., Cambridge University Press, Cambridge.

Volino, R. J., 2020, "Non-equilibrium development in turbulent boundary layers with changing pressure gradients", *Journal of Fluid Mechanics*, Vol. 897, A2.

Volino, R. J., and Schultz, M. P., 2018, "Determination of wall shear stress from mean velocity and Reynolds shear stress profiles", *Physical Review Fluids*, Vol. 3, 034606.

Volino, R. J., and Schultz, M. P., 2022, "Comparison of smooth- and rough-wall non-equilibrium boundary layers with favourable and adverse pressure gradients", *Journal of Fluid Mechanics*, Vol. 959, A35.

Wu, W., and Piomelli, U., 2018, "Effects of surface roughness on a separating turbulent boundary layer", *Journal of Fluid Mechanics*, Vol. 841, pp. 552-580.

Yoon, M., Hwang, J., Yang, J., and Sung, H. J., 2020, "Wall-attached structures of streamwise velocity fluctuations in an adverse-pressure gradient turbulent boundary layer", *Journal of Fluid Mechanics*, Vol. 885, A12.

Zagarola, M. V., and Smits, A. J., 1998, "Mean-Flow Scaling of Turbulent Pipe Flow", *Journal of Fluid Mechanics*, Vol. 373, pp. 3-79.